NANO LETTERS

Letter

pubs.acs.org/NanoLett

Lateral and Vertical Stiffness of the Epitaxial *h*-BN Monolayer on Rh(111)

Tobias Herden,[†] Markus Ternes,*[,†] and Klaus Kern[†,‡]

[†]Max Planck Institute for Solid State Research, Heisenbergstraße 1, 70569 Stuttgart, Germany

[‡]Institut de Physique de la Matière Condensée, École Polytechnique Fédérale de Lausanne (EPFL), 1015 Lausanne, Switzerland

Supporting Information

ABSTRACT: The response to strain in covalently bound single layers has a large impact on the growth and properties. We investigate the quasi-two-dimensional hexagonal boron nitride on Rh(111), which is interesting due to its high intrinsic corrugation. We use combined atomic force and scanning tunneling microscopy to measure the response of this monolayer to probing forces. Three-dimensional force maps and the atomic resolution of the layer enable us to determine lateral and vertical stiffness of this prototypical system with unprecedented spatial resolution. Extremely low stiffnesses ≈1 N/m are derived. Our experiments give insights into the mechanical properties of corrugated incommensurate layers that buckle into the third dimension to relieve strain.

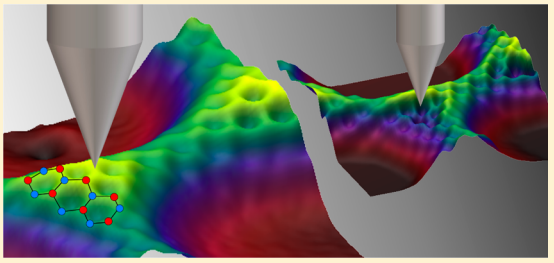

KEYWORDS: *Hexagonal boron nitride, monolayer, mechanical properties, stiffness, combined AFM/STM*

Hexagonal boron nitride (*h*-BN) consists of alternating boron and nitrogen atoms in a two-dimensional honeycomb lattice. Similar to graphene, the sp^2 hybridization creates strong covalent bonds between the atoms of a layer, while the layer as a whole is only loosely bound by van der Waals forces to adjacent layers or to supporting metal substrates.[1] The unique physical and chemical properties of *h*-BN make it an ideal dielectric material for future applications, as shown for example in graphene *h*-BN heterostructures.[2−4]

Besides the interest in *h*-BN as an insulating layer for heterostructures, *h*-BN has also been shown to be an excellent nanotemplate when grown on transition metals,[5] which electronically decouples molecules and clusters from the underlying substrate.[6−9] The mechanical properties of *h*-BN are of crucial importance to get a fundamental understanding of the mechanisms involved in the transition between commensurate and incommensurate growth,[10] the observed site-specific adsorption when deployed as template for molecules, and for possible applications in nanomechanical devices.[11] While most methods that have been employed so far, like inelastic X-ray scattering[12] or mechanical indentation experiments[13,14] average over large areas, the advances of scanning probe methods enable to detect mechanical deformations down to the picometer-scale.[15,16]

We investigate the effective stiffness of the highly corrugated *h*-BN/Rh(111)[17] as a strained model system that is perfectly accessible by combined atomic force (AFM) and scanning tunneling microscopy (STM). Well-ordered single layer *h*-BN can easily be grown on transition metal substrates by chemical vapor deposition of borazine ($B_3N_3H_6$).[1] On a Rh(111) crystal the lattice mismatch between the substrate and the *h*-BN results in a growth in which the *h*-BN monolayer forms a Moiré-like superstructure with 3.2 nm periodicity corresponding to 13 BN units on top of 12 Rh atoms.[18] Surface areas in which the nitrogen atoms of the *h*-BN are aligned with the Rh atoms of the substrate are strongly bound ("valley sites"), while areas in which the nitrogen atoms are aligned with hollow sites buckle away from the metal substrate ("rim sites") (Figure 1). This corrugation precludes a simple 2D treatment: probing the stiffness by only applying forces perpendicular to the layer, like in indentation experiments on planar sheets, neglects the effects that occur due to the corrugation. Only by investigating the stiffnesses in all spatial dimensions a full picture can be obtained.

Here we use a home-built frequency-modulated AFM with a stiff cantilever (k_0 = 1800 N/m) operating at low temperatures (T_{base} = 1.5 K) and in ultrahigh vacuum (~10^{-10} mbar). A small cantilever oscillation amplitude perpendicular to the surface of 130 pm enables us not only to detect the frequency shift Δf of the AFM cantilever from its natural resonance frequency of 18400 Hz but additionally the electrical conductance $G = I/V$ between tip and sample. This technique has two advantages: First, it allows us to use the exponential dependence of G on the tip height z to determine the absolute distance between tip apex and substrate (see Supporting Information, Figure S1). Second, the small oscillation amplitude ensures the detection of minute lateral deformations of the corrugation without averaging over large z ranges.

From sets of constant height images recorded at successively increased z we calculate the total interaction energy E and the

Received: April 11, 2014
Revised: May 13, 2014
Published: May 27, 2014

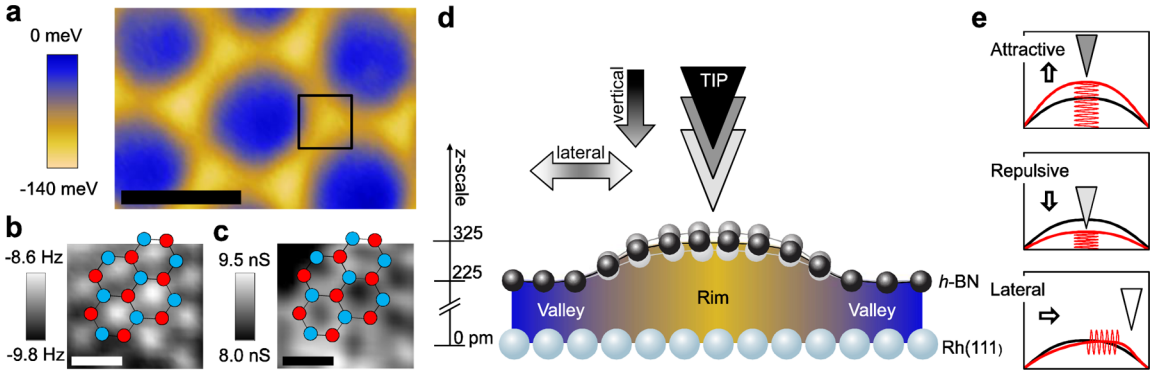

Figure 1. The *h*-BN layer and schematic concept of probing its deformation. (a) The interaction energy landscape between tip and the *h*-BN layer at z = 550 pm shows the strong corrugation of 3.2 nm periodicity. The lateral scale bar corresponds to 3 nm. (b,c) Frequency shift (b) and conductance (c) of a small region at the rim site allowing assignment of B (blue) and N (red) atoms. The lateral scale bars correspond to 0.3 nm. (d) Schematic side view of the studied system. The *h*-BN depicted by the black balls is in equilibrium position, i.e., the tip being far away (no interaction). Dark gray and light gray symbolizes the situation where the interaction between tip and *h*-BN is attractive and starting to be repulsive, respectively. The *z*-scale is based upon data extracted from DFT calculation from ref 21. (e) Model drawings of the effective stiffnesses probed in the three discussed cases of vertical attractive, vertical repulsive, and lateral attractive forces, respectively.

forces $F = -\text{grad}\ E$ acting between the probing tip and the *h*-BN layer in all spatial directions[19,20] (see methods section for details). At close tip−sample distances (z < 0.5 nm), where Pauli repulsion becomes significant, we see clear atomic contrast at the rim sites of the *h*-BN sheet in the Δf and G maps (Figure 1b, c). A maximum of G and Δf is found at the position of the atoms, becoming weaker at the interatomic center of the BN hexagons. The interaction energy difference between the atom sites and the centers of the hexagons reaches ΔE = 15 ± 5 meV at closest approach (z = 355 pm) (Figure 2a). This modulation of the total energy leads to lateral forces $F_{\parallel}$ between the tip and the *h*-BN atoms. Independent of the vertical force component $F_{\perp}$ we always find the lateral force acting on the tip to be attractive toward the atoms. In return, this causes a small decrease of the average distance between B and N atoms in the hexagon directly below the tip apex.

We determine this shift by a statistical evaluation of the distance l between the BN hexagons in the rim region (Figure 2b, c) and by a Fourier transformation of the Δf images (see Supporting Information, Figure S2 for details). We found a decrease of l by 4% for an increase in $F_{\parallel}$ from 13 to 20 pN (corresponding to a change in tip height of 67 pm). By relating the change of l to the average $F_{\parallel}$ (Figure 2d) in a first-order approximation (Hooke's law), i.e., by reducing the complex geometry of the entire rim region to a single spring (see Figure 1e) we derive an effective lateral stiffness of $k_{\parallel} = dF_{\parallel}/dl$ = 0.66 ± 0.16 N/m (Figure 2e). The main contribution of the uncertainty results from the distribution of derived distances. While mechanical layer properties are usually expressed in terms of 2D Young's moduli, we note that transferring concepts of classical mechanics is cumbersome or even impossible for such complicated and highly anisotropic systems as the corrugated *h*-BN on Rh(111).

As the lateral compression in the sheet is caused by the presence of the tip it has to be compensated for by stretching in other regions of the layer where $F_{\parallel}$ exerted by the tip is significantly weaker. Therefore, we can conclude that the derived stiffness is indeed a property of the entire rim region.

Density functional theory calculations found differences of B−N bond lengths within the superstructure of up to 4 pm due to the lattice mismatch when grown on Rh(111).[21] Our observed decrease of l at the applied forces is of the same

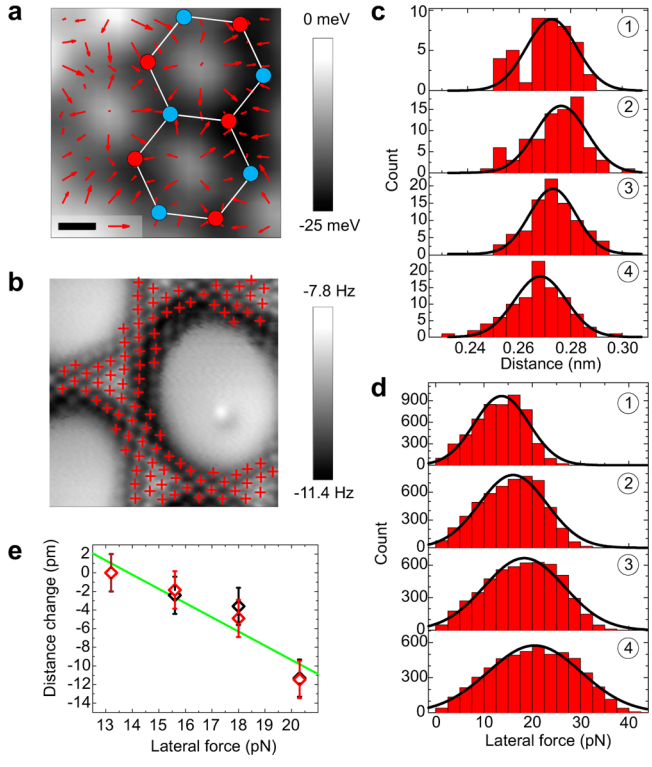

Figure 2. Lateral forces and displacement of the *h*-BN. (a) Energy landscape above the atomically resolved center of the rim recorded at a tip−sample distance z = 355 pm with an overlaid atom model. The arrows represent the lateral forces $F_{\parallel}$. Note that the forces are attractive, i.e., the tip is pulled toward the atoms. The scale bar corresponds to a distance of 0.1 nm and the reference arrow to a force of 30 pN. (b) Constant height Δf image (4 × 4 nm^2) recorded at z = 355 pm shows clear atomic contrast enabling the evaluation of the distance l to neighboring BN units at the rim sites. (c, d) Histograms of l and of $F_{\parallel}$ at z = 422, 400, 378, and 355 pm (1−4). We found l_{avg} = 278, 276, 274, and 267 pm (1−4) and $F_{\parallel,avg}$ = 13.2, 15.6, 18.0, and 20.3 pN, for decreasing z. The Gaussian fits are guides to the eye. A change of l_{avg} by 11 pm and $F_{\parallel,avg}$ by 7 pN is observed for a decrease of the tip height by 67 pm. (e) The relative shift of l_{avg} derived from the statistical analysis (black) and by FFT (red) decreases linearly with $F_{\parallel,avg}$ A linear fit (green line) enables the determination of the lateral stiffness of $k_{\parallel}$ = 0.66 ± 0.17 N/m.

dx.doi.org/10.1021/nl501349r | Nano Lett. 2014, 14, 3623−3627

magnitude, even though the deformation, which we probe originates from two effects: First, deformations within the layer, i.e. direct changes of the bond lengths below the tip apex and, second, movements of the whole rim region due to the forces applied by the tip, as depicted in Figure 1e. These two effects cannot be disentangled. Nevertheless, we want to highlight that only the achieved atomic resolution together with the spatial resolved lateral forces make a quantification of the overall movement possible. We expect this lateral flexibility to play a significant role in the frequently observed off-center adsorption of molecules on the *h*-BN.[5,9,22] The low stiffness of the entire rim region will promote topographic adaptation by the *h*-BN layer.

Besides the lateral layer deformation the presence of the tip also impacts the shape of the corrugation normal to the surface. Constant force landscapes interpolated from the vertical force component $F_\perp$ clearly show an indentation of the rim region in an area of about 6 hexagonal units of up to 25 pm at short tip−sample distances (Figure 3a, b). This apparent indentation

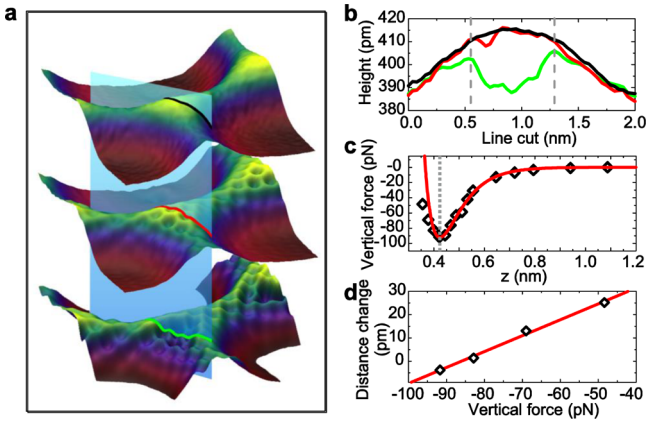

Figure 3. Deformation due to repulsive vertical forces. (a) 3D representations of constant total force landscapes (3.4 × 3.4 nm^2) at −450 pN, −575 pN, and −640 pN (top to bottom). The color code ranges from 460 to 520, 370 to 450, and 355 to 410 pm for the three images, respectively. An indentation of the layer when high forces are applied is clearly visible in the rim region. (b) The intersections (black, red, green) of the light blue plane with the force landscapes shown in (a) underlines the vertical compression, which can be estimated to be ∼25 pm of the rim site by decreasing $F_\perp$ from −575 to −640 pN. Note that the height scale corresponds to the −640 pN curve and that the −575 and −450 pN curves are offset by −30 and −100 pm, respectively. (c) The short-range forces at the rim site are fitted by a Morse type force up to z = 0.42 nm (gray dotted line), after which a significant change of slope is visible that is attributed to the pushing of the layer. (d) The difference between the fit and the data in (c) is used to deduce a vertical stiffness of $k_\perp \approx 1.5$ N/m.

cannot be solely attributed to the topographic response of the layer to the acting force, as it also includes long-range forces (electrostatic and van der Waals).[23]

To get a quantitative measure of the deformation, we focus on the distance dependence of the short-range forces by using the valley region as a reference for the long-range forces. We fit a Morse type force[24] $F = F_0[\exp(-a(z - z_0)) - \exp(-2a(z - z_0))]$ to the attractive part of the short-range forces (Figure 3c) which results in F_0 = 370 pN, a = 12 nm^{-1}, and z_0 = 0.37 nm. By interpolation of this fit we attribute the discrepancy of it and the data below z = 0.42 nm to the softness of the layer. By relating those distance changes to the acting vertical force, we find an effective stiffness of $k_\perp$ = 1.5 ± 0.6 N/m (see Supporting Information and Figure S3 for more details).

To put the effective stiffness into perspective as far as larger scale measurements that usually aim at the Young's modulus are concerned, it is worthwhile to compare our data to the measurements of ref 14. They derive the 2D elastic modulus (Y^{2D} = 200−500 GPa nm) from indentation of 1 μm diameter free few-layer *h*-BN membranes. Relating the indentation depth to the applied forces, e.g., applying our model, leads to an effective stiffness of ∼2 N/m. Hence, the stiffness that we derive for the rim regions of *h*-BN on Rh(111) is of similar magnitude as for a much larger, free membrane. (More details and a comparison to ref 16 can be found in the Supporting Information.)

At larger tip−sample distances one expects the attractive $F_\perp$ to lift the rim sites away from the supporting Rh(111) substrate. To observe this pulling we investigate the short-range forces at distances where we can neglect the Pauli repulsion (z > 0.55 nm). We observe an exponential decrease of $F_\perp$ when decreasing z as long as $F_\perp$ is above approximately −20 pN. At shorter tip−sample distances, the measured force decreases faster than the exponential fit (Figure 4a). We attribute the

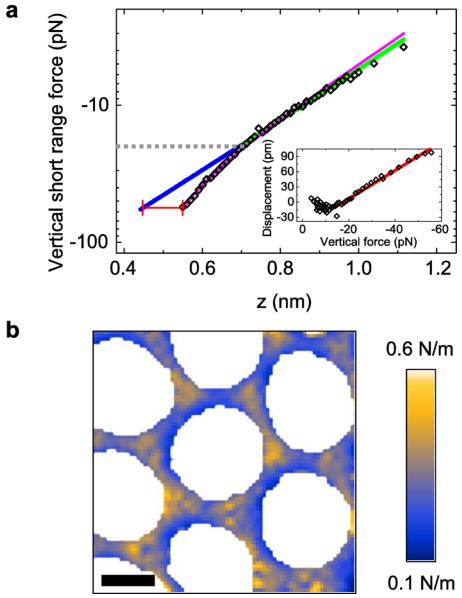

Figure 4. Deformation due to attractive vertical forces. (a) The short-range forces in the attractive regime show an over exponential increase below approximately −20 pN (gray dotted line) at the rim site, which we attribute to pulling the *h*-BN away from the surface by Δz (red bar). The exponential fit (with a decay constant of 4.2 nm^{-1}) and the interpolation below −20 pN are shown in green and blue, respectively, and the analytical function (see text) in pink. The inset shows a linear fit (red line) of the displacement against the forces from which a vertical stiffness of $k_\perp$ = 0.36 ± 0.05 N/m can be deduced. (b) The stiffness is evaluated at each point by deploying the analytical function. A Gaussian smooth of 2 × 2 pixels is applied for clarity. The scale bar corresponds to 1.5 nm.

height difference between measured force and interpolated exponential value (blue line) to a lifting of the sheet. While this evaluation requires the arbitrary cut between the exponential fit and the interpolation, we use the analytical relation $F_\perp(z) = F_0 \exp[-\kappa(z + F_\perp(z)/k_\perp)]$ (with the decay constant κ), which takes the pulling of the tip on the BN sheet at all distances into account by replacing z with $z + F_\perp(z)/k_\perp$. This equation can be

dx.doi.org/10.1021/nl501349r | *Nano Lett.* 2014, 14, 3623−3627

solved to yield $F_\perp(z) = (\kappa/k_\perp) \times W_0(F_0\kappa/k_\perp \exp[-\kappa z])$ with W_0 as the real-valued branch of the Lambert W function. We found an average of $k_\perp = 0.4 \pm 0.1$ N/m when evaluating the rim region (Figure 4b). Here again, the valley serves as a reference for the long-range forces and is not accessible by this method. As only the short-range forces are considered, the comparison against the exponential distance dependence in the investigated distance is legitimate[25,26] and consistent with the Morse type force in the repulsive regime.

Comparing our values to a classical elastostatic model of a thin shell with a single point load[27] assuming a Young's modulus of unstrained h-BN (Y = 270 GPa[28]) results in an effective stiffness of k_{CM} ~1.9 N/m (see the Supporting Information). Here we emphasize the difficulty to apply a macro-world model to our nanomechanical system. Nevertheless, even though the crude simplification of this classical model, which uses mechanical constants from unstrained h-BN is prone to fail when applied to single layers,[29] we obtain a stiffness of similar magnitude.

In summary, our experiments show how forces in all spatial dimensions in combination with atomically resolved images can be used to determine the lateral and vertical stiffness of a quasi-2D strained epitaxial system. While we show clear evidence for lateral and vertical deformation due to the forces exerted between the tip and the h-BN layer, the quantification of the stiffnesses is difficult and has a relatively large uncertainty. We found for the loosely bound rim region of the h-BN/Rh(111) very soft lateral and vertical stiffnesses in the range of 0.4−1.5 N/m. To reconsider our findings in the scope of the full system of h-BN on Rh(111), several aspects are worth highlighting: Contrary to what in-plane elastic moduli (which are orders of magnitude higher) found for mesoscopic h-BN sheets suggest, the high local lateral flexibility allows adaptation of the h-BN to quasi-commensurate growth in the valley regions. Regardless of the high residual strain, the layer grows free of dislocations and buckles in the rim regions into the observed soft superstructure. A comparison to indentation experiments reveals that the elasticity observed at the rim region is comparable to the one of free membranes[14] despite the much smaller size of only a few nanometers in the superstructure and the close proximity to the underlying Rh substrate. Recent calculations of higher-order elastic constants corroborate the softening of the h-BN monolayer when highly strained,[30] which might be key to our surprising result. Our results might motivate further investigations to elucidate the exact interplay between the mechanical, chemical, and electrical properties in such corrugated epitaxial systems.

Methods. The Rh(111) substrate is prepared by repeated cycles of Ar^+ sputtering and annealing up to 1100 K. Borazine is dosed through a leak valve for 2 min at a pressure of 1.2×10^{-6} mbar (~110 L), while the sample is kept at a temperature of approximately 1080 K. The temperature is slowly decreased to allow uniform formation of the layer before the sample is in situ transferred into the cold microscope. Two sets of 3D Δf and G data with different sizes of $8 \times 8 \times 1.3$ and $4 \times 4 \times 0.73$ nm^3 are evaluated in this work. They were obtained by taking 48 (15) 2D maps at successively increased constant tip−sample separation and at bias voltages of −0.9 (0.2) V. Vertical and lateral drift during the measurement time of up to 15 h are corrected by carefully aligning the raw Δf and G data. Interaction energy landscapes and vertical forces are calculated deploying the Sader−Jarvis method.[31] Lateral forces are determined by the gradient of the energy landscape. We assign $z \equiv 0$ as the extrapolated height, where the conductance $G(z)$ at the rim sites is equal to G_0, the quantum of conductance.[25] At −0.9 V the electrostatic forces are approximately compensated. We checked that the two sets do not differ significantly except with respect to the tip-dependent long-range forces and the resolution and that only negligible dissipation occurs during the measurement. To increase the signal-to-noise ratio, the force curves shown in Figure 3 are averaged over small discs of 0.2 nm diameter in the valley (reference for long-range forces) and at the rim. Likewise, in Figure 4, we averaged over 0.8 nm discs of six rim regions and one 1.2 nm disc for the valley reference. A more detailed description of our data processing can be found in the Supporting Information.

■ ASSOCIATED CONTENT

Supporting Information

Method details and Figures S1, S2, and S3. This material is available free of charge via the Internet at http://pubs.acs.org.

■ AUTHOR INFORMATION

Corresponding Author

*E-mail: m.ternes@fkf.mpg.de.

Notes

The authors declare no competing financial interest.

■ ACKNOWLEDGMENTS

We gratefully acknowledge discussions with L. Harnau (MPI-IS, Stuttgart) and P. Blaha (TU Vienna). Support by the SFB 767 is acknowledged.

■ REFERENCES

(1) Nagashima, A.; Tejima, N.; Gamou, Y.; Kawai, T.; Oshima, C. *Phys. Rev. B* **1995**, *51*, 4606−4613.

(2) Britnell, L.; Gorbachev, R. V.; Jalil, R.; Belle, B. D.; Schedin, F.; Mishchenko, A.; Georgiou, T.; Katsnelson, M. I.; Eaves, L.; Morozov, S. V.; Peres, N. M. R.; Leist, J.; Geim, A. K.; Novoselov, K. S.; Ponomarenko, L. A. *Science* **2012**, *335* (6071), 947−950.

(3) Levendorf, M. P.; Kim, C.-J.; Brown, L.; Huang, P. Y.; Havener, R. W.; Muller, D. A.; Park, J. *Nature* **2012**, *488* (7413), 627−632.

(4) Kim, S. M.; Hsu, A.; Araujo, P. T.; Lee, Y.-H.; Palacios, T.; Dresselhaus, M.; Idrobo, J.-C.; Kim, K. K.; Kong, J. *Nano Lett.* **2013**, *13* (3), 933−941.

(5) Dil, H.; Lobo-Checa, J.; Laskowski, R.; Blaha, P.; Berner, S.; Osterwalder, J.; Greber, T. *Science* **2008**, *319* (5871), 1824−1826.

(6) Goriachko, A.; He, Y.; Knapp, M.; Over, H.; Corso, M.; Brugger, T.; Berner, S.; Osterwalder, J.; Gerber, T. *Langmuir* **2007**, *23*, 2928.

(7) Berner, S.; Corso, M.; Widmer, R.; Groening, O.; Laskowski, R.; Blaha, P.; Schwarz, K.; Goriachko, A.; Over, H.; Gsell, S.; Schreck, M.; Sachdev, H.; Greber, T.; Osterwalder, J. *Angew. Chem.* **2007**, *46*, 5115.

(8) Bose, S.; García-García, A. M.; Ugeda, M. M.; Urbina, J. D.; Michaelis, C. H.; Brihuega, I.; Kern, K. *Nat. Mater.* **2010**, *9*, 550.

(9) Kahle, S.; Deng, Z.; Malinowski, N.; Tonnoir, C.; Forment-Aliaga, A.; Thontasen, N.; Rinke, G.; Le, D.; Turkowski, V.; Rahman, T. S.; Rauschenbach, S.; Ternes, M.; Kern, K. *Nano Lett.* **2012**, *12* (1), 518−521.

(10) Woods, C. R.; Britnell, L.; Eckmann, A.; Ma, R. S.; Lu, J. C.; Guo, H. M.; Lin, X.; Yu, G. L.; Cao, Y.; Gorbachev, R. V.; Kretinin, A. V.; Park, J.; Ponomarenko, L. A.; Katsnelson, M. I.; Gornostyrev, Y. N.; Watanabe, K.; Taniguchi, T.; Casiraghi, C.; Gao, H. J.; Geim, A. K.; Novoselov, K. S. *arXiv* **2014**, 1401.2637v2.

(11) Mashoff, T.; Pratzer, M.; Geringer, V.; Echtermeyer, T. J.; Lemme, M. C.; Liebmann, M.; Morgenstern, M. *Nano Lett.* **2010**, *10* (2), 461−465.

(12) Bosak, A.; Serrano, J.; Krisch, M. *Phys. Rev. B* **2006**, *73*, 041402R.
(13) Lee, C.; Wei, X.; Kysar, J. W.; Hone, J. *Science* **2008**, *321* (5887), 385−388.
(14) Song, L.; Ci, L.; Lu, H.; Sorokin, P. B.; Jin, C.; Ni, J.; Kvashnin, A. G.; Kvashnin, D. G.; Lou, J.; Yakobson, B. I.; Ajayan, P. M. *Nano Lett.* **2010**, *10* (8), 3209−3215.
(15) Hauptmann, N.; Mohn, F.; Gross, L.; Meyer, G.; Frederiksen, T.; Berndt, R. *New J. Phys.* **2012**, *14*, 073032.
(16) Koch, S.; Stradi, D.; Gnecco, E.; Barja, S.; Kawai, S.; Diaz, C.; Alcami, M.; Martin, F.; Lopes Vazquez de Parga, A.; Miranda, R.; Glatzel, T.; Meyer, E. *ACS Nano* **2013**, *7* (4), 2927−2934.
(17) Corso, M.; Auwärter, W.; Muntwiler, M.; Tamai, A.; Greber, T.; Osterwalder, J. *Science* **2004**, *303*, 217.
(18) Laskowski, R.; Blaha, P.; Gallauner, T.; Schwarz, K. *Phys. Rev. Lett.* **2007**, *98*, 106802.
(19) Hölscher, H.; Langkat, S. M.; Schwarz, A.; Wiesendanger, R. *Appl. Phys. Lett.* **2002**, *81*, 4428.
(20) Ternes, M.; Lutz, C. P.; Hirjibehedin, C. F.; Giessibl, F. J.; Heinrich, A. J. *Science* **2008**, *319*, 1066.
(21) Diaz, J. G.; Ding, Y.; Koitz, R.; Seitsonen, A. P.; Iannuzzi, M.; Hutter, J. *Theor. Chem. Acc.* **2013**, *132*, 1350−1366.
(22) Natterer, F. D.; Patthey, F.; Brune, H. *Phys. Rev. Lett.* **2012**, *109*, 066101.
(23) We note that constant Δf images, as usually obtained by noncontact AFM, also cannot be used unequivocally for this analysis because Δf is rather a measure of the force gradient than of the tip−sample interaction force.[32]
(24) Morse, P. M. *Phys. Rev.* **1929**, *34*, 57−64.
(25) Ternes, M.; Gonzalez, C.; Lutz, C. P.; Hapala, P.; Giessibl, F. J.; Jelínek, P.; Heinrich, A. J. *Phys. Ref. Lett.* **2011**, *106*, 016802.
(26) Sugimoto, Y.; Ondráček, M.; Abe, M.; Pou, P.; Morita, S.; Perez, R.; Flores, F.; Jelínek, P. *Phys. Rev. Lett.* **2013**, *111*, 106803.
(27) Geckeler, J. W. *Handbuch der Physik*; Geiger, H., Scheel, K., Eds.; Julius Springer: Berlin, 1928; pp 141−308.
(28) Nag, A.; Raidongia, K.; Hembram, K. P. S. S.; Datta, R.; Waghmare, U. V.; Rao, C. N. R. *ACS Nano* **2010**, *4* (3), 1539−1544.
(29) Zhang, D.-B.; Akatyeva, E.; Dumitrică, T. *Phys. Rev. Lett.* **2011**, *106*, 255503.
(30) Peng, Q.; Ji, W.; De, S. *Comput. Mater. Sci.* **2012**, *56* (0), 11−17.
(31) Sader, J. E.; Jarvis, S. P. *Appl. Phys. Lett.* **2004**, *84* (10), 1801−1803.
(32) Giessibl, F. J. *Appl. Phys. Lett.* **2001**, *78* (1), 123−125.